Quantitative Investigation of Inter-Crystal Scatter and Penetration in the GE Discovery RX PET/CT Scanner using Monte Carlo Simulations

Navid Zeraatkar, Mohammad R. Ay, *Member, IEEE*, Saeed Sarkar, Parham Geramifar, and Arman Rahmim *Member, IEEE*

Abstract– **As the dimensions of crystal elements in modern PET systems is getting smaller, the fraction of events undergoing inter-crystal scattering (ICS) and penetration increases. This has deteriorative impact on the spatial resolution of images. However, with the utilization of statistical image reconstruction methods in PET, compensation for ICS and penetration impacts is feasible by accurately modeling their effects in the projection space. We aim to perform such a work for the GE Discovery RX (DRX) PET/CT system. In this work, we investigated ICS and penetration in the DRX for acquiring a quantitative view of their respective contributions. We analyzed the events in the form of coincidences instead of single photons. Also as a novelty, we discriminated between the origins of the event mispositiong. For this, we applied the GATE (Geant4 Application for Tomographic Emission) Monte Carlo toolkit and used our previously validated model of DRX. Numerous points in different positions were analyzed inside the field of view (FOV) of DRX. Finally, using geometrical symmetries of the DRX and interpolation, the fraction of ICS and penetration could be determined for all possible positions inside the FOV. The results revealed that the notable variations in quantitative behavior of ICS and penetration occurred with varying radial positions; the fraction of ICS/penetration-induced mispositioned coincidences out of true coincidences ranged from 28.7% at the center to 57.8% at the edge of the transaxial FOV. This comprehensive quantification of ICS and penetration not only provides a deeper understanding of their respective contributions, but is also aimed to be utilized in refining the system matrix in the image reconstruction task to achieve resolution modeling in the scanner.**

This work was supported by the Research Center for Science and Technology in Medicine under grant No. 88.256.

Navid Zeraatkar is with the Research Center for Science and Technology in Medicine, Tehran University of Medical Sciences, Tehran, Iran (e-mail: navid_zeraatkar@yahoo.com).

Mohammad Reza Ay is with the Department of Medical Physics and Biomedical Engineering, Tehran University of Medical Sciences, Tehran, Iran and Research Center for Science and Technology in Medicine, Tehran, Iran, and Research Institute for Nuclear Medicine, Tehran University of Medical Sciences, Tehran, Iran (e-mail: mohammadreza_ay@tums.ac.ir).

Saeed Sarkar is with the Department of Medical Physics and Biomedical Engineering, Tehran University of Medical Sciences, Tehran, Iran and Research Center for Science and Technology in Medicine, Tehran, Iran.

Parham Geramifar is with the Faculty of Physics and Nuclear Engineering, Amir Kabir University of Technology and Research Center for Science and Technology in Medicine, Tehran, Iran, and Research Institute for Nuclear Medicine, Tehran University of Medical Sciences, Tehran, Iran.

Arman Rahmim is with the Department of Radiology, Johns Hopkins Medical Institutions, Baltimore, Maryland, USA (e-mail: arahmim1@jhmi.edu).

I. Introduction

While there is continuing demand for higher resolution in PET systems, technological improvements are still challenged by the presence of inter-crystal scatter (ICS) and inter-crystal penetration phenomena in detectors [1]. Penetration (exhibiting itself in the form of the so-called parallax effect) occurs when a photon passes through a crystal on which it is incident with no interaction and is instead detected in another crystal. The penetration effect is therefore probable only for photons entering the crystal at non-perpendicular angles and intensifies as the photon energy increases and/or the attenuation coefficient of the detector material decreases. Hence, the probability of a 511-keV photon in a PET system for penetrating through the incident crystal with no interaction is considerable. In the other hand, ICS can be present even for photons incident perpendicularly to the crystal and happens when a photon escapes from the crystal it initially entered after one or more Compton interactions and hence deposits some of its energy in one or more crystals other than the initial crystal. Fig. 1 depicts an example of a photon experiencing ICS and penetration in a typical detector block. Both ICS and penetration have deteriorative impact on spatial resolution of PET scanners because they cause some photons to be detected in crystals not corresponding to the position of the annihilation from which the photon emitted. The consequence of this photon mispositioning is that the coincidences in which at least one of the two photons mispositioned due to ICS or penetration are likely registered in incorrect line of responses (LORs). In addition, the current trend of PET detection system implementation that leans toward fabrication of smaller crystals for reaching better intrinsic spatial resolution worsens the impact of ICS and penetration due to the higher probability of the photon escape from the prime crystal before interaction or after Compton interaction.

Nonetheless, following the introduction and utility of statistical image reconstruction methods in PET, and the so-called system matrix, it has been shown that it is possible to

compensate for ICS and penetration by accurately modeling their effects within the projection space [2-6]. In contrast to conventional post-reconstruction partial volume correction (PVC), this approach can be viewed as reconstruction-based PVC [7]. An understanding of the quantitative behavior of ICS and penetration plays an important role whether in design of a more optimized PET detection system or in more accurate modeling of ICS and penetration effects for modification of system matrix in order to enhance the quality of reconstructed images.

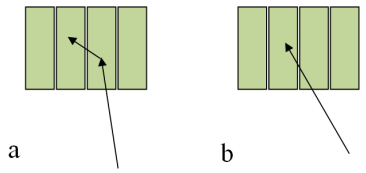

Fig. 1. An example of a photon experiencing (a) ICS and (b) penetration in a typical detector block.

To the best of our knowledge, up to now the studies performed on quantification of ICS and inter-crystal penetration have primarily (and even merely) concentrated on single 511-keV photons instead of considering coincidences [8-11]. By contrast, PET detection systems are based on coincidences and therefore a single-photon-based study may not provide sufficient measurements due to the fact that singles (single photons detected in contrast to coincidences) by themselves are not of importance; the coincidences arranged in LORs are meaningful for the purpose of image reconstruction. Hence, it is more meaningful to assess the impact of ICS and penetration on the mispositioning of coincidences. In this work, we analyzed the quantity of ICS and penetrated events in the form of coincidences in the PET subsystem of GE Discovery RX (DRX). Foremost, as a novel study, we discriminated between penetrated events and ICS events. Since discrimination of ICS and penetrated events is not feasible practically, Monte Carlo (MC) approaches are considered the most reliable ones for this aim. In order to do this, we employed GATE (Geant4 Application for Tomographic Emission) MC toolkit [12] and used our previously validated models of DRX [13].

II. Materials and Methods

A. Monte Carlo Model of DRX PET Subsystem

As mentioned earlier, we used our previously validated MC models [13] in this work.

DRX follows block-detector structure in which arrays of subunits (so-called modules) are repeated. Modules, being subunits of the blocks, are composed from an array of crystal elements.

The crystal dimensions in DRX are $4.2 \times 6.3 \times 30$ mm^3, while they are repeated 9×6 times in transaxial and axial directions respectively to form a module. An array of 2×4 modules in respectively transaxial and axial directions builds a block. Replication of 35 blocks around an 88.6 cm-diameter ring composes the DRX detection system. Furthermore, axial and transaxial field of view (FOV) of the DRX are nominally 15.7 cm and 70 cm, respectively. The crystal material is Cerium-doped Lutetium Yttrium Orthosilicate (LYSO). The coincidence window in the GATE MC model was set to 5.85 ns. The lower and upper energy thresholds were adjusted to 425 keV and 650 keV, respectively. In addition, the shielding of the scanner, the inter-crystal septa, and the electronic properties of the readout system were taken into account in the modeling [13-19]. The detection system characteristics of DRX are summarized in Table I.

TABLE I. The Detection System Characteristics of DRX

Crystal material	LYSO
Crystal pitch (axial)	6.4 mm
Crystal pitch (transaxial)	4.3 mm
Crystal depth	30 mm
No. of crystals per module	9 x 6
No. of modules per detector block	2 x 4
No. of detector blocks	35
No. of rings	24
No. of crystals per ring	630
Ring diameter	88.6 cm
Axial FOV	15.7 cm
Transaxial FOV	70 cm

B. Discrimination of ICS and penetration

There are multiple factors that restrict the spatial resolution in PET by causing the coincidences to be registered in incorrect LORs regarding to the position of the positron emission. Positron range, photons non-collinearity, Compton scattering of photons in FOV, and random coincidences are of those factors. In addition, ICS and penetration, which were explained before, severely cause mispositioning of the coincidences.

Although the discrimination of the mispositioned coincidences is hardly possible in practice by repetition of a point source scanning in numerous FOV positions, there is no straightforward approach for determination of the factor causing the mispositioning practically. Nonetheless, MC simulation coupled with an intelligent post-processing algorithm provided us with this ability. For this, in our simulation we employed an ideal 511-keV point source (i.e. dimensionless and free from positron range and photons non-collinearity). In addition, we evaluated the entirety of the FOV with no extended attenuating medium so that no scattering was possible inside FOV. Finally, before data analysis, we deleted all random coincidences from the database. Consequently, the only factor resulting in coincidence mispositioning was ICS and/or penetration (ICS-P).

Ultimately, in-house software was developed for discrimination and categorization of different types of coincidences stored in output file of GATE after every simulation. Fig. 2 shows the classification we considered for

the coincidences. For distinguishing mispositioned coincidences from those which were correctly registered as true coincidences (purely true coincidences), the in-house software examined each true coincidence to identify whether the spatial volume composed from two corresponding pixels of the two singles (so-called volume of response (VOR)) encompasses the known position of the point source or not. If the point source was inside the VOR, it meant that the coincidence was purely true; otherwise it was mispositioned because of ICS-P. Furthermore, regarding to the subject that GATE registers the number of Compton interactions of every single of the coincidence in the detector crystals before being stopped or escaping (in the form of so-called *comp_det* variable), we categorized the mispositioned coincidences into three groups based on three possible conditions for comp_det variables of the singles in a coincidence (including both zero, both non-zero, and one zero and the other non-zero); we named them group-1, group-2, and group-3. In this way, if the dual single events were ONLY affected (one or both) by penetration, the coincidence was sorted in group-1. If one single event was affected by ICS (possibly including penetration), and the other was not affected by ICS (i.e. affected by penetration or no mispositioning at all), the coincidence was categorized into group-2. Finally, group-3 was dedicated to coincidences whose both singles affected by ICS (possibly also including penetration). Although at the first glance, this kind of categorization may seem confusing or even useless, it can be beneficial for different analyses. For instance, group-1 represents the coincidences mispositioned because of penetration and free from ICS.

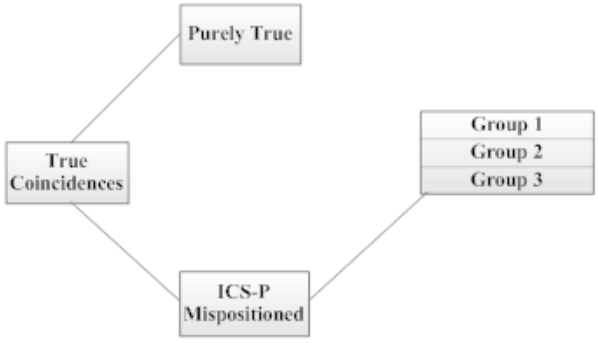

Fig. 2. Schematic of the proposed classification of the true coincidences.

C. Monte Carlo simulations

The best way to quantitatively analyze ICS and penetration in the whole FOV, as accurate as possible, is to sample all possible positions inside FOV via simulated point sources. Nevertheless, such a work takes too much time for both simulation and process in addition to huge volumes of generated data. In order to overcome this issue, we decided to take advantage of geometrical symmetries of the scanners and acquire the critical direction(s) along which quantitative behavior of ICS and penetration was notable, though the same as previously reported studies [4, 5] the expectation was to observe the most significant variations in radial direction. For this, we performed some simulations in finite numbers of positions and then processed the data. As mentioned earlier, the DRX detection system consists of 35 blocks. It can be seen in Fig. 3.a that the geometry of the DRX is generated by repeating a block together with its shown corresponding angle ($\gamma = 10.29^{\circ}$) around a 360-degree ring. So by obtaining the behavior of ICS and penetration in one angular interval (shaded region), one can extend the behavior to the entire 360-degree ring. Nonetheless, there was no symmetry in the radial direction. Therefore, for obtaining a better understanding of the quantitative behavior of ICS and penetration along radial direction, numerous radial positions were investigated to have enough samples in order to correctly estimate the behavior of ICS and penetration. Therefore, the more radial positions were investigated from ICS and penetration point of view, the better understanding of their quantitative behavior in radial direction was provided. According to the cylindrical shape of the system, the two halves of the DRX in the axial direction are symmetrical. Hence, having the behavior of ICS and penetration in one axial half, the behavior can be extended for the other half. The positions of the points at axial center sampled in angular and radial directions are illustrated in Fig. 3.a. Also, the axial and radial offsets of the positions assessed in one half of axial direction are shown in Fig. 3.b. For angular analysis, six points at axial center and radius of 20 cm were assessed (Fig 3.a) starting from -4.83˚ to 5.45˚ by angular steps of 2.06˚. For axial analysis, five axial positions in one half of the cylinder were chosen ranging from the axial center (z = 0 mm) to approximately the edge of axial FOV (z = 73.75 mm). In each of these steps, four radial positions (0 cm, 5 cm, 20 cm, and 35 cm) were investigated from ICS and penetration point of view. Finally, since there was no symmetry in the radial direction, and also because it was expected that the most significant variations of either qualitative or quantitative behavior of ICS and penetration occurs in this direction, we assessed numerous radial positions at the axial center.

III. Results

The processing of output data of MC simulation was performed using the aforementioned in-house software after each data acquisition. Since we aimed to evaluate the proportion of coincidence events undergone ICS-P, the quantity of ICS and penetration was calculated in terms of the percentage of the true coincidences mispositioned because of ICS-P.

Fig. 4.a shows the proportion of the ICS-P coincidences to true coincidences in an angular period (10.29˚) at axial center and the radius of 20 cm in the DRX. As it can be seen, the quantitative variations of the triple groups and consequently ICS-P coincidences are really negligible in angular direction. Fig. 4.b illustrates the quantity of ICS-P at four different radii

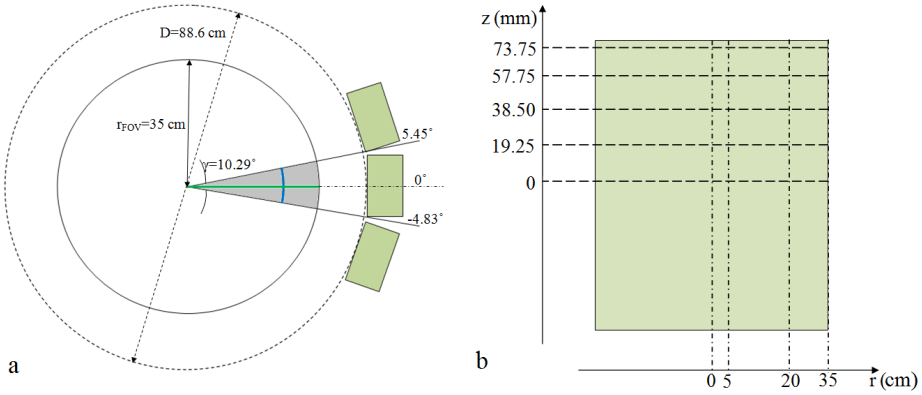

Fig. 3. (a) Cross section of the DRX gantry in which the green line and the blue arc are the locus of points assessed in radial direction and angular direction, respectively; (b) Top view of the DRX gantry in which the locus of investigated points in axial direction are shown. The dimensions in Z-direction are exaggerated.

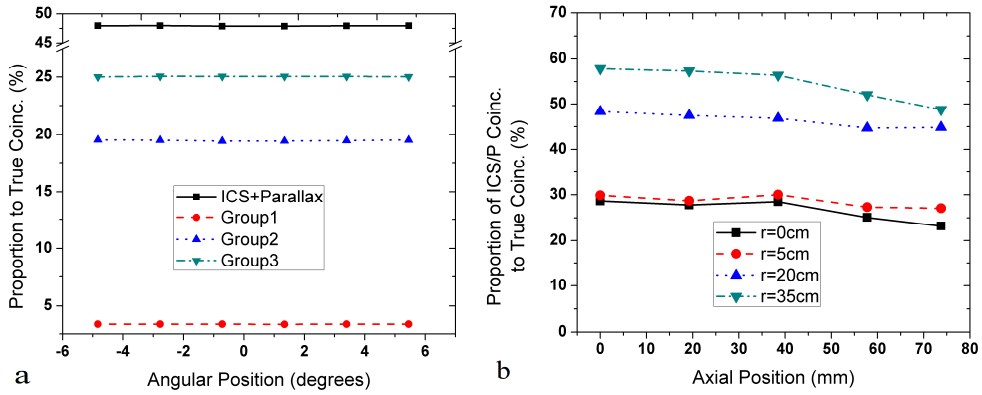

Fig. 4. The proportion of ICS-P coincidences to true coincidences in DRX (a) along the angular direction in one angular period at radius of 20 cm; and (b) along the axial direction at four different radial positions.

along axial direction in the DRX. The ideal condition with no variation along axial direction happened if the axial extent of the scanner was infinite. But in practice, the straighter are the lines in Fig. 4.b, the more homogeneous is the quantitative behavior of ICS-P along the axial direction. As it can be seen in Fig. 4.b, the variations of ICS-P along with axial position at middle radii (5 cm and 20 cm) are less than 5%.

In addition, the quantitative trends of the triple groups and the total ICS-P coincidences along radial direction are illustrated in Fig. 5.

IV. Discussion

Fig. 4.a reveals that the quantitative behavior of the ICS and penetration in DRX is almost constant with variation of angular position. Since the full ring is composed from replication of 35 angular regions and the behavior of ICS and penetration in each region is the same, it is evident that the quantity of ICS-P coincidences along the whole 360-degree ring is constant for each radial position. So no necessity is seen for allocating time to assess the ICS-P coincidences quantity in angular direction not only in the case of the DRX but also for other scanners that have a similar geometry to the DRX's.

In addition, Fig. 4.b shows that the proportion of ICS-P coincidences to true coincidences in the DRX slightly decreases as the source gets more distant from the axial center (z = 0 mm) and closer to the edge of the axial FOV. The reason is that with respect to the characteristic of coincidence detection, as the source travels from the axial center towards the axial FOV edge, the range of probable angles[1] for annihilation photons to be detected as a coincidence becomes tighter. Hence, the probability of the photons for undergoing penetration (and also ICS) becomes smaller as the source gets closer to the edge of the axial extent. Lashkari et al [10], using MC simulation, have shown that the increment of the incident 511-keV photon angle from 0˚ to 10˚ results in about 3% increase in the percentage of ICS for a single in a $4\times4\times20\,mm^3$-crystal array. Likewise, supposing that the probability of a perpendicular photon for penetration is zero, the increment of the photon angle from 0˚ to 10˚ causes about 35% increase in the percentage of penetrated single photons [10]. As it is evident from Fig. 4.b, since the quantity of ICS-P coincidences is larger at greater radii, its variation along axial position is also more rigorous.

[1]The angle between the photon trajectory and the normal vector of the crystal surface

Fig. 5 proves that while conventional theoretical explanations may expect that the amount of ICS-P is minimal at center of transaxial FOV (r = 0), the minimum may happen at other radii, because the scanner is composed of blocks of detectors in which all the subcrystals are not oriented toward the center. Instead, each block is oriented toward the center. So expecting that the photons emitting from a source at the center have perpendicular angles with all the crystals is not true. This issue causes the minimum point for ICS-P amount to happen in a different radius (depending on the scanner geometry) rather than the center. Furthermore, as it can be seen in Fig. 5, at the center, the value of group-1, that indicates the amount of the penetration-induced mispositioned coincidences, is not zero. This can be justified by two reasons: firstly, the non-ideal orientation of the crystals toward the center as described earlier, and secondly, the fact that the data acquisition performed in 3-dimensional (3D) mode. The 3D mode causes the emitted photons from a source to have non-perpendicular angles with the crystals in the other detector rings that leads to a non-zero probability for penetration.

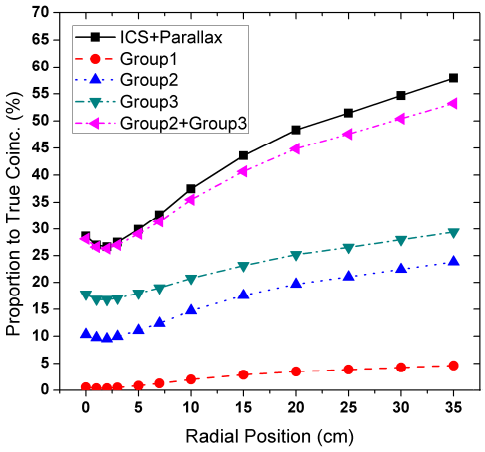

Fig. 5. The proportion of ICS-P and the triple groups coincidences to true coincidences along radial direction in DRX.

V. Conclusion

It is concluded that the most rigorous variations of ICS-P quantity in the DRX occurs along radial direction. Furthermore, fluctuation of ICS-P amount along the angular direction can be considered as nearly constant in that direction. Likewise, ICS-P quantity has slight yet observable variations along the axial direction. This comprehensive quantification of ICS and penetration not only provided a deeper understanding of them, but also we aim to use them for modification of the system matrix and therefore to achieve resolution modeled image reconstruction for the DRX scanner.

References

[1] A. Rahmim and H. Zaidi, "PET versus SPECT: strengths, limitations and challenges," *Nucl Med Commun,* vol. 29, pp. 193-207, Mar 2008.

[2] J. Qi, R. M. Leahy, S. R. Cherry, A. Chatziioannou, and T. H. Farquhar, "High-resolution 3D Bayesian image reconstruction using the microPET small-animal scanner," *Phys Med Biol,* vol. 43, pp. 1001-13, 1998.

[3] V. Y. Panin, F. Kehren, H. Rothfuss, D. Hu, C. Michel, and M. E. Casey, "PET Reconstruction With System Matrix Derived From Point Source Measuremnts," *IEEE Transactions on Nuclear Science,* vol. 53, pp. 152-159, Feb 2006.

[4] V. Y. Panin, F. Kehren, C. Michel, and M. E. Casey, "Fully 3-D PET Reconstruction With System Matrix Derived From Point Source Measurements," *IEEE Transactions on Medical Imaging,* vol. 25, pp. 907-921, Jul 2006.

[5] A. M. Alessio, P. E. Kinahan, and T. K. Lewellen, "Modeling and Incorporation of System Response Functions in 3-D Whole Body PET," *IEEE Transactions on Medical Imaging,* vol. 25, pp. 828-837, Jul 2006.

[6] A. Rahmim, J. Tang, M. A. Lodge, S. Lashkari, M. R. Ay, R. Lautamaki, B. M. Tsui, and F. M. Bengel, "Analytic system matrix resolution modeling in PET: an application to Rb-82 cardiac imaging," *Phys Med Biol,* vol. 53, pp. 5947-65, Nov 7 2008.

[7] O. G. Rousset, A. Rahmim, A. Alavi, and H. Zaidi, "Partial volume correction strategies in PET.," *PET Clinics,* vol. 2, pp. *235-249*, 2007.

[8] Y. Shao, S. R. Cherry, S. Siegel, and R. W. Silverman, "A Study of Inter-Crystal Scatter in Small Scintillator Arrays Designed for High Resolution PET Imaging," *IEEE Transactions on Nuclear Science,* vol. 43, pp. 1938-1944, Jun 1996.

[9] E. Yoshida, K. Kitamura, Y. Kimura, F. Nishikido, K. Shibuya, T. Yamaga, and H. Murayama, "Inter-crystal scatter identification for a depth-sensitive detector using support vector machine for small animal positron emission tomography," *Nucl. Instrum. Methods A,* vol. 571, pp. 243-246, 2007.

[10] S. Lashkari, S. Sarkar, M. R. Ay, and A. Rahmim, "The influence of crystal material on intercrystal scattering and the parallax effect in PET block detectors: a Monte Carlo study," in *Biomed 2008*, 2008, pp. 633-636.

[11] S. Rechka, R. Fontaine, R. Lecomte, and M. Rafecas, "LabPET inter-crystal scatter study using gate," in *IEEE Nuclear Science Symposium Conference Record (NSS/MIC)*, Orlando, FL, 2009, pp. 3988-3994.

[12] S. Jan, G. Santin, D. Strul, S. Staelens, K. Assie, D. Autret, S. Avner, R. Barbier, M. Bardies, P. M. Bloomfield, D. Brasse, V. Breton, P. Bruyndonckx, I. Buvat, A. F. Chatziioannou, Y. Choi, Y. H. Chung, C. Comtat, D. Donnarieix, L. Ferrer, S. J. Glick, C. J. Groiselle, D. Guez, P. F. Honore, S. Kerhoas-Cavata, A. S. Kirov, V. Kohli, M. Koole, M. Krieguer, D. J. van der Laan, F. Lamare, G. Largeron, C. Lartizien, D. Lazaro, M. C. Maas, L. Maigne, F. Mayet, F. Melot, C. Merheb, E. Pennacchio, J. Perez, U. Pietrzyk, F. R. Rannou, M. Rey, D. R. Schaart, C. R. Schmidtlein, L. Simon, T. Y. Song, J. M. Vieira, D. Visvikis, R. Van de Walle, E. Wieers, and C. Morel, "GATE: a simulation toolkit for PET and SPECT," *Phys Med Biol,* vol. 49, pp. 4543-61, Oct 7 2004.

[13] P. Geramifar, M. R. Ay, M. Shamsaie, G. Loudos, and A. Rahmim, "Monte Carlo based performance assessment of four Commercial GE Discovery PET/CT scanners using GATE," in *IEEE Nuclear Science Symposium Conference Record*, Dresden, Germany, 2008, pp. 3995-99.

[14] GE-Healthcare, "Discovery RX 16 Product Data," 2006.

[15] B. J. Kemp, C. Kim, J. J. Williams, A. Ganin, and V. J. Lowe, "NEMA NU 2-2001 performance measurements of an LYSO-based PET/CT system in 2D and 3D acquisition modes," *J Nucl Med,* vol. 47, pp. 1960-7, Dec 2006.

[16] H. Baghaei, O. Mawlawi, Y. Wang, H. Li, R. Ramirez, S. Kim, Y. Zhang, T. Pan, J. Liu, S. Liu, and W.-H. Wong, "A Comparison of Five Whole-Body PET Scanners by Scanning Hoffman Brain

Phantom," in *IEEE Nuclear Science Symposium Conference Record*, 2006, pp. 1973-1976.

[17] M. Teras, T. Tolvanen, J. J. Johansson, J. J. Williams, and J. Knuuti, "Performance of the new generation of whole-body PET/CT scanners: Discovery STE and Discovery VCT," *Eur J Nucl Med Mol Imaging,* vol. 34, pp. 1683-92, Oct 2007.

[18] GE-Healthcare, "Discovery STE 8 Product Data," 2006.

[19] P. Geramifar, M. R. Ay, M. Shamsaii Zafarghandi, G. Loudos, and A. Rahmim, "Monte Carlo simulation of the GE LYSO-based Discovery RX PET/CT scanner using GATE: a validation study," in *Annual Congress of the Europe. Assoc. Nucl. Med. (ENAM), abstract 296*, 2008.